



HAL
open science

p-adaptation using residual distribution schemes with continuous finite elements

Rémi Abgrall, Heloise Beaugendre, Cecile Dobrzynski, Quentin Viville

► **To cite this version:**

Rémi Abgrall, Heloise Beaugendre, Cecile Dobrzynski, Quentin Viville. p-adaptation using residual distribution schemes with continuous finite elements. [Research Report] RR-8808, Inria Bordeaux Sud-Ouest; IMB; Bordeaux INP. 2015. hal-01225583

HAL Id: hal-01225583

<https://inria.hal.science/hal-01225583>

Submitted on 6 Nov 2015

HAL is a multi-disciplinary open access archive for the deposit and dissemination of scientific research documents, whether they are published or not. The documents may come from teaching and research institutions in France or abroad, or from public or private research centers.

L'archive ouverte pluridisciplinaire **HAL**, est destinée au dépôt et à la diffusion de documents scientifiques de niveau recherche, publiés ou non, émanant des établissements d'enseignement et de recherche français ou étrangers, des laboratoires publics ou privés.



p -adaptation using residual distribution schemes with continuous finite elements

R. Abgrall, H. Beaugendre, C. Dobrzynski , Q. Viville

**RESEARCH
REPORT**

N° 8808

November 2015

Project-Team CARDAMON



p -adaptation using residual distribution schemes with continuous finite elements

R. Abgrall*, H. Beaugendre[†], C. Dobrzynski[‡], Q. Viville[§]

Project-Team CARDAMON

Research Report n° 8808 — November 2015 — 34 pages

Abstract: In this paper, a novel approach that allows to use p -adaptation with continuous finite elements is proposed. Under certain conditions, primarily the use of a residual distribution scheme, it is possible to avoid the continuity constraint imposed to the approximate solution, while still retaining the advantages of a method using continuous finite elements. The theoretical material, the complete numerical method and practical results show as a proof of concept that p -adaptation is possible with continuous finite elements, well suited for non linear cases and that this approach brings some advantages.

Key-words: p -adaptation, Continuous and discontinuous finite elements, Residual distribution scheme, Linear equations, Non linear equations

* Institut für Mathematik, Universität Zürich, Winterhur Strasse 190, CH-8057 Zürich.

[†] Univ. Bordeaux, IMB, UMR 5251, F-33400, Talence, France; CNRS, IMB, UMR 5251, F-33400, Talence, France; Bordeaux INP, IMB, UMR 5251, F-33400, Talence, France; INRIA, F-33400 Talence, France.

[‡] Univ. Bordeaux, IMB, UMR 5251, F-33400, Talence, France; CNRS, IMB, UMR 5251, F-33400, Talence, France; Bordeaux INP, IMB, UMR 5251, F-33400, Talence, France; INRIA, F-33400 Talence, France.

[§] Univ. Bordeaux, IMB, UMR 5251, F-33400, Talence, France; CNRS, IMB, UMR 5251, F-33400, Talence, France; INRIA, F-33400 Talence, France.

**RESEARCH CENTRE
BORDEAUX – SUD-OUEST**

200 avenue de la Vieille Tour
33405 Talence Cedex

p-adaptation avec éléments finis continus pour les schémas aux résidus

Résumé : On présente dans ce rapport de recherche une nouvelle approche qui permet d'utiliser la *p*-adaptation avec des éléments finis continus. On montre que sous certaines conditions, en particulier l'utilisation d'un schéma aux résidus distribués, il est possible d'éviter la contrainte de continuité imposée à la solution discrète, tout en conservant les avantages d'une méthode utilisant des éléments finis continus. L'étude théorique, le schéma numérique complet, ainsi que les résultats numériques obtenus démontrent qu'il est possible d'appliquer la *p*-adaptation aux éléments finis continus, que cette méthode présente certains avantages et fonctionne avec des équations non linéaires.

Mots-clés : *p*-adaptation, éléments finis continus et discontinus, schémas aux résidus, équations non linéaires

Contents

1	Introduction	3
2	Mathematical problem and residual distribution schemes	5
2.1	Basic notions of residual distribution schemes	5
2.2	Some particular residual distribution schemes	7
2.2.1	The SUPG scheme	7
2.2.2	The Lax-Wendroff scheme	7
2.2.3	The Rusanov scheme	8
2.3	Construction of a high order monotonicity preserving Residual Distribution scheme	8
2.3.1	Limitation	8
2.3.2	Stabilization	9
2.4	Boundary conditions	9
2.5	A Lax-Wendroff like theorem and its consequences	9
3	Residual distribution schemes and p-adaptation	10
3.1	Example of a triangle and quadratic interpolation	11
3.2	Definition of a new nodal residual	12
4	Application of p-adaptation to residual distribution schemes: practical implementation	13
4.1	Nodal residuals	13
4.2	Global Jacobian	14
4.3	Boundary conditions	14
4.4	Coincidence of quadrature formula	14
5	Numerical test cases using p-adaptation	14
5.1	Lax-Wendroff scheme - Subsonic test case	14
5.2	Lax-Friedrichs scheme - Transonic test case	15
5.2.1	Shock capturing term	15
5.2.2	Shock detector and p-adaptation	16
5.2.3	Shock width, oscillations and p-adaptation	16
5.3	Supersonic test case	20
6	Extension to three dimensions	20
6.1	3D p-adaptation with quadratic tetrahedra	24
6.2	Bézier basis functions	25
6.3	Hypersonic three dimensional test case	27
7	Conclusion	27
	Appendix A Implicit numerical solver	28

1 Introduction

Because of their potential in delivering higher accuracy with lower cost than low order methods, high-order methods for computational fluid dynamics (CFD) have obtained considerable attention in the past two decades [25]. By high order, we mean third order or higher. Most industrial codes used today for CFD simulations are based upon second-order finite volume

methods (FVM), finite difference methods (FDM), or finite element methods (FEM) [25]. As second-order methods are used in most CFD codes, some very complex flows simulations might remain out of their reach. Indeed, in some cases, second-order methods are still too much dissipative and as a consequence they require much finer meshes and become too expensive even on modern supercomputer clusters. In order to deal with a large and diverse range of problems, lots of researches have been conducted with the aim of designing robust and stable high order methods, see [16] and [23]. High-order methods allow the use of coarser meshes [25, 23, 24], high-order boundary representation [20], and improve the accuracy of the solutions [25, 23, 12]. Because of their potential, we believe that the next generation of CFD solvers will have to be based upon high order methods. Besides the use of higher order methods, a very promising approach is the use of hp-adaptation to change locally the order of accuracy and the size of the mesh according to the solution [19].

Among high-order methods, the Discontinuous Galerkin (DG) method [18, 9, 15, 22] and the Residual Distribution (RD) method [6, 1, 4, 14, 5], have had a growing interest in the recent years. The DG method has a compact stencil regardless the order of the polynomials representing the solution [17]. This very local formulation leads to a great flexibility, especially for the parallelization of its implementation. However, DG methods suffer from the rapid increase of the number of degrees of freedom (dof) [11], and then, simulations in three-dimensional space may quickly become too expensive. A possible way to overcome this problem is to use p -adaptation [10] (which is conceptually easy with DG methods), where the local approximation order p (hence the term p -adaptation) is dictated by the flow field. The optimal solution is hp -adaptation (mesh and polynomial adaptations) to achieve the best accuracy with the minimum cost. In smooth regions, p -adaptation is preferred, whereas in discontinuous regions, h -adaptation is preferred.

Another possible approach is the class of residual distribution schemes. RD methods have a longer experience in stabilization mechanisms and shock capturing abilities than DG schemes [21]. Moreover, RD methods offer a very compact stencil like DG methods, but with a smaller number of degrees of freedom [6]. The drawback is that to achieve this low number of degrees of freedom, the continuity of the approximation is required, and consequently, the use of p -adaptation with continuous finite elements is a priori not possible as this would violate the continuity requirement. The aim of this work is to demonstrate that it is indeed possible to use p -adaptation with continuous finite elements in the frame of RD schemes. Such an approach, while offering the same advantages of classical residual distribution schemes (like among others the low number of degrees of freedom, the non-oscillatory behavior and the accuracy on smooth problems [6]), exhibits some interesting advantages thanks to p -adaptation, like an improved convergence and better shock capturing abilities. With this approach, we can in some way benefit from some of the properties usually exclusive to either the class of continuous or discontinuous methods. To the best of our knowledge, the approach presented here is new. The practical implementation of p -adaptation for RD scheme results in a CFD solver that can use high order elements in smooth regions, and low order elements in discontinuous regions. In this sense, this approach is following the recommendations for the next generation of CFD solvers [25].

The paper is organized as follows: in section 2, the mathematical problem is defined and we recall briefly the general principles of the Residual Distribution schemes. In section 3, we expose how it is theoretically possible to use p -adaptation in order to redefine the nodal residual, and in section 4, this new nodal residual is used to construct the proposed residual distribution scheme. Some numerical results are presented in section 5, along with some benefits brought by p -adaptation. The extension to 3D test cases is discussed in section 6. In conclusion, we invoke some possible future extensions and developments to the work presented here.

2 Mathematical problem and residual distribution schemes

2.1 Basic notions of residual distribution schemes

In this section, the basic notions of RD schemes are summarized, more details can be found in [6]. We are interested in the numerical approximation of steady hyperbolic problems of the form

$$\operatorname{div} \mathbf{F}(\mathbf{U}) = 0, \tag{1}$$

where $\mathbf{U} : \Omega \subset \mathbb{R}^d \rightarrow \mathbb{R}^p$ is the vector of p conservative variables, Ω is an open set of \mathbb{R}^d , $d = 2, 3$, and $\mathbf{F} = (f_1, \dots, f_d)$ is the vector of flux functions, with $f_i(\mathbf{U}) : \Omega \rightarrow \mathbb{R}^p$, $i = 1, \dots, d$.

Dirichlet boundary conditions are weakly imposed on the inflow boundary [13]:

$$\partial\Omega^- = \{x \in \partial\Omega, \mathbf{n} \cdot \nabla_u \mathbf{F} < 0\}, \tag{2}$$

where \mathbf{n} is the outward normal.

The target exemple we are interested in here is the Euler equations with the vector of unknowns

$$\mathbf{U} = \begin{pmatrix} \rho \\ \rho \mathbf{u} \\ E \end{pmatrix}, \quad \mathbf{F} = \begin{pmatrix} \rho \mathbf{u} \\ \rho \mathbf{u} \otimes \mathbf{u} + p \operatorname{Id}_{d \times d} \\ (E + p) \mathbf{u} \end{pmatrix}$$

where ρ is the density, \mathbf{u} is the fluid velocity, E is the total energy, i.e. the sum of the internal energy e and the kinetic energy, and p is the pressure. The system is closed with an equation of state, $p = p(e, \rho)$, the function p satisfies standard convexity assumption, and here we deal with the simplest case, i.e. we assume a perfect gas equation of state,

$$p = (\gamma - 1)e,$$

with $\gamma = 1.4$. In this setting, the vector of unknowns is such that $\mathbf{U} \in \mathbb{R}^{2+d}$, with $\rho > 0$ and $e > 0$. On solid boundaries, we impose weakly no slip boundary conditions.

In this section, the discussion will stay rather general, and we will not focus particularly on the Euler system, but a general hyperbolic system. We want to find an approximate solution to equations (1)-(2) in the continuous finite element space $Z_h = \{\mathbf{U}_h \in C^0(\Omega)^p; \forall K \in \mathcal{T}_h, \mathbf{U}_h|_K \in \mathbb{P}^k(K)^p\}$, $k \in \mathbb{N}^*$. The tessellation \mathcal{T}_h of Ω covers it,

$$\Omega = \bigcup_{K \in \mathcal{T}_h} K =: \Omega_h, \tag{3}$$

where a generic element is denoted by K . We also assume that the tessellation is conformal. We denote by $\mathcal{D} = \{\sigma_j\}$ the set of degrees of freedom.

Remark 2.1 *In this paper, all the numerical applications will be made with triangular or tetrahedral elements, but can be extended to quad and hex. Other kind of simplices has not been checked.*

For practical applications, it is important to define the basis of the vector space $\mathbb{P}^k(K)$. A natural choice is made by the Lagrange basis. Another choice that will be useful in this work is the Bézier basis. In the case of triangular and tetrahedral elements, we denote by λ_l the \mathbb{P}^1 Lagrange basis. Any point \mathbf{x} of \mathbb{R}^2 or \mathbb{R}^3 can be characterized by its barycentric coordinates: $(\lambda_j(\mathbf{x}))_{j=1, d+1}$. The Lagrange points of degree k are the points of K with barycentric coordinates $(i_1/(k), \dots, i_p/(k), \dots, i_{d+1}/(k))$ with i_l an integer such that $\sum_{l=1}^{d+1} i_l = k$ and $i_l \geq 0$. This defines the degrees of freedom in the Lagrange case.

In the Bézier case, we consider the same degrees of freedom associated to the polynomials

$$B_{i_1, \dots, i_{d+1}} = \binom{k}{i_1, \dots, i_{d+1}} \lambda_1^{i_1} \dots \lambda_p^{i_p} \dots \lambda_{d+1}^{i_{d+1}}.$$

Clearly, they sum to unity and are positive on K .

We note φ_h the basis functions (Lagrange or Bézier) associated to the degrees of freedom. The approximate solution \mathbf{U}_h is thus written as

$$\mathbf{U}_h = \sum_{\sigma_j \in \mathcal{D}} \mathbf{U}_j \varphi_j.$$

In the Lagrange case, $\mathbf{U}_j = \mathbf{U}_h(\sigma_j)$. We can now write the discrete equations of the residual distribution scheme. They are described by means of residuals that are defined for each degree of freedom of any element, and they must satisfy the following rules:

1. If σ is an internal degree of freedom, we write

$$\forall \sigma \in \mathcal{T}_h \cap \Omega, \sum_{K, \sigma \in K} \Phi_\sigma^K = 0,$$

where the split residuals Φ_σ^K must satisfy the conservation constraint:

$$\forall \sigma \in K, \sum_{\sigma \in K} \Phi_\sigma^K = \Phi^K \quad (4)$$

where we have introduced the total residual:

$$\Phi^K := \int_{\partial K} \mathbf{F}(\mathbf{U}_h) \cdot \mathbf{n} \, dx \quad (5)$$

2. If σ is a degree of freedom on the boundary $\partial\Omega$, we also introduce the boundary residuals Φ_σ^Γ . They satisfy the following conservation relation:

$$\forall \Gamma \subset \partial\Omega, \sum_{\sigma \in \Gamma} \Phi_\sigma^\Gamma = \int_{\partial\Gamma} \left(\mathcal{F}(\mathbf{U}_h, \mathbf{U}_-, \mathbf{n}) - \mathbf{F}(\mathbf{U}^h) \cdot \mathbf{n} \right) dx \quad (6)$$

where \mathcal{F} is a numerical flux that depends on the boundary condition \mathbf{U}_- , the outward normal \mathbf{n} and the local state \mathbf{U}_h . Similarly, we define Φ^Γ by:

$$\Phi^\Gamma := \int_{\partial\Gamma} \left(\mathcal{F}(\mathbf{U}_h, \mathbf{U}_-, \mathbf{n}) \mathbf{F}(\mathbf{U}_h) \cdot \mathbf{n} \right) dx \quad (7)$$

And finally the residual distribution scheme writes:

$$\forall \sigma \in \mathcal{T}_h, \sum_{K, \sigma \in K} \Phi_\sigma^K + \sum_{\Gamma, \sigma \in \Gamma} \Phi_\sigma^\Gamma = 0. \quad (8)$$

Before going further, let us give some examples of residual distribution schemes.

2.2 Some particular residual distribution schemes

2.2.1 The SUPG scheme

It is defined by:

$$\Phi_\sigma^{K,SUPG} = \int_K \varphi_\sigma \operatorname{div} \mathbf{F}(\mathbf{U}_h) dx + h_K \int_K (A \cdot \nabla \varphi_\sigma) \Xi (A \cdot \nabla \mathbf{U}_h) dx. \quad (9)$$

The term A represents $A = (A_1, \dots, A_d)$ where A_j is the Jacobian of the j -th component of the flux. As it is quite traditional, we have set

$$A \cdot \nabla \varphi = \sum_{j=1}^d A_j \frac{\partial \varphi}{\partial x_j}.$$

Using the Green-Gauss formula, it can be rewritten in a more suitable form for conservation problems:

$$\begin{aligned} \Phi_\sigma^{K,SUPG} &= - \int_K \nabla \varphi_\sigma \cdot \mathbf{F}(\mathbf{U}_h) dx + \int_{\partial K} \varphi_\sigma \mathbf{F}(\mathbf{U}_h) \cdot \mathbf{n} \\ &\quad + h_K \int_K (A \cdot \nabla \varphi_\sigma) \Xi (A \cdot \nabla \mathbf{U}_h) dx. \end{aligned}$$

and we note that the term $\int_{\partial K} \varphi_\sigma \mathbf{F}(\mathbf{U}_h) \cdot \mathbf{n}$ can actually be dropped in the calculations thanks to the continuity of \mathbf{U}_h .

In (9), the matrix Ξ is a parameter, and we usually take the matrix defined by its inverse:

$$\Xi^{-1} = \sum_{j=1}^{d+1} (A \cdot \varphi_j)^+.$$

Whatever the degree of our approximation, this matrix is formulated in \mathbb{P}^1 and since K is a simplex, the matrix is defined using $d + 1$ points (the vertices).

Clearly,

$$\sum_{\sigma_j \in K} \Phi_\sigma^{K,SUPG} = \int_{\partial K} \mathbf{F}(\mathbf{U}_h) \cdot \mathbf{n},$$

so that the conservation relation (4) is satisfied.

2.2.2 The Lax-Wendroff scheme

The Lax-Wendroff scheme is a simplified version of the SUPG scheme,

$$\Phi_\sigma^{K,lw} = \frac{\Phi_\sigma^K}{N_{dof}^K} + \int_{\Omega_K} (A \cdot \nabla \varphi_\sigma) \Xi (A \cdot \nabla \mathbf{U}_h) dx \quad (10)$$

Here, N_{dof}^K is the number of degrees of freedom in K . Again,

$$\sum_{\sigma \in K} \Phi_\sigma^{K,lw} = \int_{\partial K} \mathbf{F}(\mathbf{U}_h) \cdot \mathbf{n}.$$

2.2.3 The Rusanov scheme

This scheme is a generalisation of the 1D Rusanov scheme. We define

$$\Phi_\sigma^{K,Rus} = \frac{\Phi^K}{N_{dof}^K}(\mathbf{U}_h) + \frac{1}{N_{dof}^K} \alpha^K \sum_{\sigma_j \in K} (\mathbf{U}_\sigma - \mathbf{U}_{\sigma_j}). \quad (11)$$

The parameter α^K is chosen as to be larger than the maximum of the spectral radii of the matrix $A \cdot \nabla \varphi_\sigma$. In the scalar case, this choice guarantees that the scheme satisfies a local maximum principle. In the system case, it is proved to be non oscillatory and very dissipative.

2.3 Construction of a high order monotonicity preserving Residual Distribution scheme

If the flow is smooth, we can use the Lax-Wendroff-like scheme presented above. However, when the solution present discontinuities, special care has to be taken to handle them. We recall in the following what we do.

2.3.1 Limitation

We present here the construction a high order residual distribution scheme starting from the first order Rusanov scheme of section 2.2.3. We choose the Rusanov scheme as it is essentially the one we use in our numerical experiments, notably for its shock capturing abilities (see section 5). The method is presented in [2], where several other examples are considered. In practice, the construction is achieved through the following sequence of operations.

The nodal residuals of (11) are first projected on the left eigenvectors L_n obtained from the Jacobian matrices evaluated at the arithmetic average state $\bar{\mathbf{U}}$, in the direction $\mathbf{n} = \frac{\mathbf{u}}{\|\mathbf{u}\|}$ (the mean velocity vector of the fluid).

The intermediate nodal residuals then write:

$$\Phi_\sigma^{K,*} = L_n \Phi_\sigma^{K,Rus}, \quad (12)$$

and

$$\Phi^{K,*} = \sum_{\sigma \in K} \Phi_\sigma^{K,Rus}. \quad (13)$$

Then, the high order distribution coefficients are computed from the original first order distribution coefficients by the non linear mapping:

$$\hat{\beta}_\sigma^{K,*} = \frac{\left(\frac{\Phi_\sigma^{K,*}}{\Phi^{K,*}} \right)^+}{\sum_{\sigma_j \in K} \left(\frac{\Phi_{\sigma_j}^{K,*}}{\Phi^{K,*}} \right)^+} \quad (14)$$

Now we can compute the high order nodal residuals in the characteristic space:

$$\hat{\Phi}_\sigma^{K,*} = \hat{\beta}_\sigma^{K,*} \Phi^{K,*}, \quad (15)$$

and finally, we project them from the characteristic space to the physical space

$$\hat{\Phi}_\sigma^K = R_n \hat{\Phi}_\sigma^{K,*} \quad (16)$$

where R_n are the right eigenvectors.

2.3.2 Stabilization

The solution obtained with a Rusanov scheme can exhibit spurious modes and can show poor iterative convergence [6]. These problems are solved via the addition of the filtering term presented above for the schemes (9) and (10), and so the high order filtered Rusanov scheme for the Euler equations read:

$$\widehat{\Phi}_\sigma^{K,Rus}(\mathbf{U}_h) = \widehat{\Phi}_\sigma^K(\mathbf{U}_h) + \theta \int_{\Omega_K} (A \cdot \nabla \varphi_\sigma) \Xi (A \cdot \nabla \mathbf{U}_h) dx \quad (17)$$

where θ is a shock capturing term. In most applications, we take $\theta = 1$, and in some cases a more elaborated version must be chosen. In this paper, we always choose the shock capturing term, equation (32), in order to simplify the text.

2.4 Boundary conditions

For the degrees of freedom lying on the boundary of the domain, we use the following formula for the nodal residuals:

$$\forall \Gamma \subset \partial\Omega, \quad \Phi_\sigma^\Gamma(\mathbf{U}_h) = \int_\Gamma \varphi_\sigma (\mathcal{F}(\mathbf{U}_h, \mathbf{U}_-, \mathbf{n}) - \mathbf{F}(\mathbf{U}_h) \cdot \mathbf{n}) dx. \quad (18)$$

where \mathbf{U}^Γ is the state that is imposed by the Dirichlet conditions. In the case of a no-slip condition, the state \mathbf{U}^Γ satisfies this state, and the numerical flux is only a pressure flux. See [13] for more details.

2.5 A Lax-Wendroff like theorem and its consequences

The following theorem has been proved in [7]:

Theorem 2.2 *Assume the family of meshes $\mathcal{T} = (\mathcal{T}_h)_h$ is regular. For K an element or a boundary element of \mathcal{T}_h , we assume that the residuals $\{\Phi_\sigma^K\}_{\sigma \in K}$ satisfy:*

- *For any $M \in \mathbb{R}^+$, there exists a constant C which depends only on the family of meshes \mathcal{T}_h and M such that for any $\mathbf{U}_h \in Z_h$ with $\|\mathbf{U}_h\|_\infty \leq M$, then*

$$\|\Phi_\sigma^K(u_{h|K})\| \leq C \sum_{\sigma, \sigma' \in K} |\mathbf{U}_\sigma - \mathbf{U}_{\sigma'}| \quad (19)$$

- *They satisfy the conservation property (4)-(5).*

Then if there exists a constant C_{max} such that the solutions of the scheme (8) satisfy $\|\mathbf{U}_h\|_\infty \leq C_{max}$ and a function $\mathbf{V} \in L^2(\Omega)^p$ such that $(\mathbf{U}_h)_h$ or at least a sub-sequence converges to \mathbf{V} in $L^2(\Omega)^p$, then \mathbf{V} is a weak solution of (1).

One of the interests of this result, besides indicating automatic consistency constraints for a scheme (8), is that the important constraint is to have the conservation relations (4)-(5) *at the element level*. This is a weaker statement than the usual one: usually, we ask conservation at the element interface level, and not *globally* on the element. Note that (4)-(5) enables however to explicitly construct the numerical flux, so that the scheme (4)-(5) can be reinterpreted as an almost standard finite volume scheme, see [3] for more details. Of course there is something to pay: the flux needs to be genuinely multidimensional.

Let us take a closer look at the relation (4)-(5). We need to see how they are actually implemented. Indeed, in the computer implementation, we do not ask for (4)-(5), but for a discrete counterpart of these relations, namely:

For any element $K \subset \Omega_h$,

$$\sum_{\sigma \in K} \Phi_{\sigma}^K(\mathbf{U}_h) = \oint_{\partial K} \mathbf{F}(\mathbf{U}_h) \cdot \mathbf{n} \quad (20a)$$

and any boundary element $\Gamma \subset \partial\Omega_h$,

$$\sum_{\sigma \in \Gamma} \Phi_{\sigma}^{\Gamma} = \oint_{\Gamma} (\mathcal{F}(\mathbf{U}_h, \mathbf{U}_-, \mathbf{n}) - \mathbf{F}(\mathbf{U}_h) \cdot \mathbf{n}) dx \quad (20b)$$

where \oint denotes the use of a quadrature formula, which reads:

1. On elements:

$$\oint_{\partial K} \mathbf{F}(\mathbf{U}_h) \cdot \mathbf{n} = \sum_{e \text{ edge/face } \subset \partial K} \left(|e| \sum_q \omega_q \mathbf{F}(\mathbf{U}_q) \cdot \mathbf{n} \right)$$

2. On boundary elements:

$$\oint_{\Gamma} (\mathcal{F}(\mathbf{U}_h, \mathbf{U}_-, \mathbf{n}) - \mathbf{F}(\mathbf{U}_h) \cdot \mathbf{n}) dx = |\Gamma| \sum_q \omega_q (\mathcal{F}(\mathbf{U}_q, \mathbf{U}_-, \mathbf{n}) - \mathbf{F}(\mathbf{U}_q) \cdot \mathbf{n})$$

If we have a close look at the proof of theorem 2.2, we see that besides the boundedness of the sequences of solution in suitable norms that enable to use compactness argument, what really matters at the algebraic level is that we have the following property on any edge:

If $\Gamma = \Gamma'$ is the same face shared by respectively the two adjacent elements K and K' , then we have $\mathbf{n}_{\Gamma} = -\mathbf{n}_{\Gamma'}$ and consequently:

$$\int_{\Gamma} \varphi_{\sigma} \mathbf{F}(\mathbf{U}_h) \cdot \mathbf{n} + \int_{\Gamma'} \varphi_{\sigma} \mathbf{F}(\mathbf{U}_h) \cdot \mathbf{n} = 0, \quad (21)$$

where $\varphi_{\sigma} \in \mathbb{P}^k(K)$ is the basis function associated to the degree of freedom σ in K .

This is clearly true because \mathbf{U}_h is continuous. Now, in the implementation, the easiest way to do so is that the quadrature points on Γ seen from K are the same as the ones on Γ seen from K' .

These two remarks are at the core of the present development, as we see now.

3 Residual distribution schemes and p-adaptation

As we have seen in the previous section, what matters for conservation is that, for any element K , the sum of the residuals is equal to the total residual, or more precisely:

$$\sum_{\sigma \in K} \Phi_{\sigma}^K = \oint_{\partial K} \mathbf{F}(\mathbf{U}_h) \cdot \mathbf{n}.$$

The total residual $\Phi^K = \oint_{\partial K} \mathbf{F}(\mathbf{U}_h) \cdot \mathbf{n}$ is obtained thanks to quadrature formulas. We show in this section that in many cases this quantity can be rewritten as a weighted sum of total residuals on sub-elements. To make this more precise, we look at the quadratic case on a triangle, where the Simpson formula is used on each edge. The main idea of this paper comes from this observation along with a way of using it.

3.1 Example of a triangle and quadratic interpolation

Let us now consider the case of a triangular element and a quadratic interpolation.

We consider a triangle; to simplify its vertices are denoted by 1,2,3 and the mid-points of the edges are denoted by 4,5,6 (see fig. 1).

We subdivide the triangle $K = (1, 2, 3)$ into four sub-triangles: $K_1 = (1, 4, 6)$, $K_2 = (4, 2, 5)$, $K_3 = (5, 3, 6)$ and $K_4 = (4, 5, 6)$, as shown in fig.1. If we denote by $\lambda_i, i = 1, 2, 3$ the barycentric coordinates corresponding respectively to the vertices $i = 1, 2, 3$ then the linear interpolant of the flux \mathbf{F} is

$$\mathbf{F}^{(1)} = \sum_{i=1}^3 \mathbf{F}(\mathbf{U}_i)\lambda_i$$

and the quadratic interpolant of the same flux is

$$\mathbf{F}^{(2)} = \sum_{i=1}^6 \mathbf{F}(\mathbf{U}_i)\varphi_i$$

with:

$$\begin{aligned} \varphi_i &= (2\lambda_i - 1)\lambda_i, & \text{for } i = 1, 2, 3 \\ \varphi_4 &= 4\lambda_2\lambda_1, & \varphi_5 = 4\lambda_3\lambda_2, & \varphi_6 = 4\lambda_1\lambda_3. \end{aligned}$$

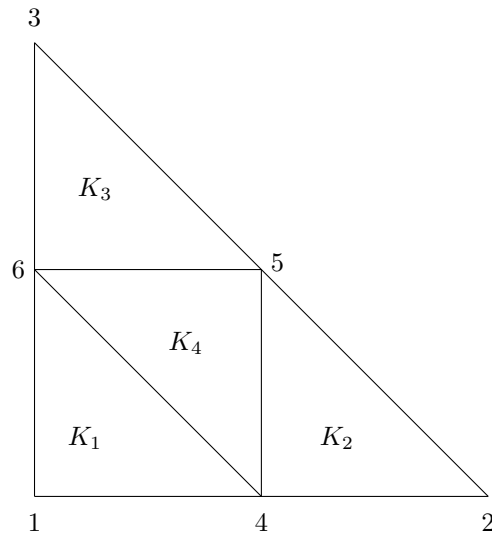


Figure 1: Subdivided triangle K .

Let us evaluate the total residual for the quadratic interpolant, we denote by \mathbf{n}_i the integral

$\int_K \nabla \lambda_i dx$, $i = 1, 2, 3$ and we have:

$$\begin{aligned}
\int_K \operatorname{div} \mathbf{F}^{(2)} dx &= \int_K \sum_{i=1}^6 (\mathbf{F}_x(\mathbf{U}_i) \frac{\partial \varphi_i}{\partial x} + \mathbf{F}_y(\mathbf{U}_i) \frac{\partial \varphi_i}{\partial y}) dx \\
&= \sum_{i=1}^6 \int_K \mathbf{F}(\mathbf{U}_i) \cdot \nabla \phi_i dx \\
&= \sum_{i=1}^6 \mathbf{F}(\mathbf{U}_i) \cdot \int_K \nabla \phi_i dx \\
&= \sum_{i=1}^3 \mathbf{F}(U_i) \frac{\mathbf{n}_i}{3} + \frac{4}{3} ((\mathbf{F}(U_4)(\mathbf{n}_1 + \mathbf{n}_2) + \mathbf{F}(U_5)(\mathbf{n}_2 + \mathbf{n}_3) \\
&\quad + \mathbf{F}(U_6)(\mathbf{n}_1 + \mathbf{n}_3)) \\
&= \frac{2}{3} (\mathbf{F}(U_1) \frac{\mathbf{n}_1}{2} + \mathbf{F}(U_4) \frac{\mathbf{n}_2}{2} + \mathbf{F}(U_6) \frac{\mathbf{n}_3}{2}) \\
&\quad + \frac{2}{3} (\mathbf{F}(U_4) \frac{\mathbf{n}_1}{2} + \mathbf{F}(U_2) \frac{\mathbf{n}_2}{2} + \mathbf{F}(U_5) \frac{\mathbf{n}_3}{2}) \\
&\quad + \frac{2}{3} (\mathbf{F}(U_6) \frac{\mathbf{n}_1}{2} + \mathbf{F}(U_5) \frac{\mathbf{n}_2}{2} + \mathbf{F}(U_3) \frac{\mathbf{n}_3}{2}) \\
&\quad - 2(\mathbf{F}(U_5) \frac{\mathbf{n}_1}{2} + \mathbf{F}(U_6) \frac{\mathbf{n}_2}{2} + \mathbf{F}(U_4) \frac{\mathbf{n}_3}{2}) \\
&= \frac{2}{3} \left(\int_{K_1} \operatorname{div} \mathbf{F}^{(1)} dx + \int_{K_2} \operatorname{div} \mathbf{F}^{(1)} dx \right. \\
&\quad \left. + \int_{K_3} \operatorname{div} \mathbf{F}^{(1)} dx \right) + 2 \int_{K_4} \operatorname{div} \mathbf{F}^{(1)} dx
\end{aligned} \tag{22}$$

where $\mathbf{F}^{(1)}$ denotes the \mathbb{P}^1 interpolant of the flux in each of the sub-triangles of figure 1. The change in signs comes from the fact that the inward normals of the sub-triangle K_4 , appearing in the expression of $\int_{K_4} \operatorname{div} \mathbf{F}^{(1)} dx$, are the opposite of the vectors $(\mathbf{n}_i/2)$.

The relation (22) demonstrates that a very simple relation, with positive weights, exists between the \mathbb{P}^1 residuals in the sub-triangles and the quadratic residual in K .

Similar formulas can be found for \mathbb{P}^3 triangles and can be generalized to higher orders and to 3-dimensional elements.

3.2 Definition of a new nodal residual

With the relation (22) we are able to redefine the nodal residuals, keeping the constraint that

$$\sum_{i \in K} \Phi_\sigma^K = \int_{\partial K} \mathbf{F}^{(2)} \cdot \mathbf{n} \tag{23}$$

For this purpose we first need to define the nodal residuals inside sub-divided elements in such a way that (23) is still satisfied.

We prove that if the conservation constraint (4)-(5) is imposed on the nodal residuals of the sub-elements, then naturally the conservation constraint (23) is satisfied. We give the proof for triangular elements, it can be generalized to other types of elements.

With ξ a sub-element of the triangle K , ($\xi = K_1, \dots, K_4$), we impose the conservation constraint inside ξ :

$$\sum_{\sigma \in \xi} \Phi_{\sigma}^{\xi} = \int_{\partial \xi} \mathbf{F}^{(1)} \cdot \mathbf{n} \quad (24)$$

where $\mathbf{F}^{(1)}$ is the \mathbb{P}^1 interpolant of the flux $\mathbf{F}(\mathbf{U}_{\sigma})$ with σ the degrees of freedom of ξ .

From relation (22), we can write:

$$\int_{\partial K} \mathbf{F}^{(2)} \cdot \mathbf{n} \, dx = \sum_{\xi=K_1, K_2, K_3, K_4} \gamma_{\xi} \int_{\partial \xi} \mathbf{F}^{(1)} \cdot \mathbf{n} \quad (25)$$

where $\gamma_{\xi} = 2/3$ or 2 and $\mathbf{F}^{(2)}$ is the \mathbb{P}^2 interpolant of $\mathbf{F}(\mathbf{U}_{\sigma})$ with σ the degrees of freedom of K .

The idea is to define Φ_{σ}^K by:

$$\Phi_{\sigma}^K = \sum_{\xi \ni \sigma} \gamma_{\xi} \Phi_{\sigma}^{\xi}. \quad (26)$$

Thanks to relations (24) and (26), the conservation relation (23) still holds:

$$\begin{aligned} \sum_{\sigma \in K} \Phi_{\sigma}^K &= \sum_{\sigma \in K} \left(\sum_{\xi \ni \sigma} \gamma_{\xi} \Phi_{\sigma}^{\xi} \right) \\ &= \sum_{\xi} \gamma_{\xi} \left(\sum_{\sigma \in \xi} \Phi_{\sigma}^{\xi} \right) \\ &= \sum_{\xi} \gamma_{\xi} \int_{\partial \xi} \mathbf{F}^{(1)} \cdot \mathbf{n} \\ &= \int_{\partial K} \mathbf{F}^{(2)} \cdot \mathbf{n} \, dx \end{aligned}$$

We can remark that it is possible to use any scheme inside the elements ξ as long as they satisfy the conservation relation (24) and the nodal residuals in K are defined by relation (26).

Under the assumption of the Lax-Wendroff theorem, the new scheme with arbitrary mixed \mathbb{P}^1 and \mathbb{P}^2 elements to compute the residuals will also be convergent to a weak solution of the problem because the conservation property (4) is still satisfied (see [4]).

4 Application of p-adaptation to residual distribution schemes: practical implementation

Now we need to make the distribution schemes presented in Section 2.2 compatible with the p -adaptation concepts presented in Section 3.

4.1 Nodal residuals

For the computation of the nodal residuals in a subdivided element, we use the formula (26) and thus we have:

$$\Phi_{\sigma}^{K, \xi} = \alpha_{\xi} \times \Phi_{\sigma}^{\xi} \quad (27)$$

where we denote $\Phi_{\sigma}^{K, \xi}$ the contribution of the node σ in triangle K computed in the sub-triangle ξ of K .

4.2 Global Jacobian

In practice, to solve the residual distribution scheme, we use an implicit numerical solver, see Appendix A for more details. To compute the global Jacobian of the RD scheme, for example in the case of the Lax-Wendroff scheme, equation (10), we need to differentiate the two terms of (10):

$$\frac{\partial \Phi_\sigma^\xi(\mathbf{U}_h)}{\partial \mathbf{U}_j} = \frac{1}{N_{dof}^\xi} \frac{\partial}{\partial \mathbf{U}_j} \left(\Phi^\xi(\mathbf{U}_h) + \int_\xi A \cdot \nabla \varphi_\sigma \Xi A \cdot \nabla \mathbf{U}_h dx \right) \quad (28)$$

and so, according to (26), we have:

$$\frac{\partial \Phi_\sigma^{K,\xi}(\mathbf{U}_h)}{\partial \mathbf{U}_j} = \alpha_\xi \times \frac{\partial \Phi_\sigma^\xi(\mathbf{U}_h)}{\partial \mathbf{U}_j}. \quad (29)$$

4.3 Boundary conditions

In the residual distribution schemes, the nodal residuals of boundary faces are computed using formula (18).

Let Γ be a face of a subdivided element K lying on the boundary of Ω . The face Γ is therefore subdivided into sub-faces; let ς be such a sub-face. From formula (26), we see that in order to be consistent with relation (18) in the case of subdivision, we need to multiply the nodal residuals of the subdivided boundary by the sub-division coefficient of the element containing this sub-divided boundary face:

$$\Phi_\sigma^{\Gamma,\varsigma} = \alpha_\xi \times \Phi_\sigma^\varsigma \quad (30)$$

and thus the contribution to the global Jacobian writes:

$$\frac{\partial \Phi_\sigma^{\Gamma,\varsigma}(\mathbf{U}_h)}{\partial \mathbf{U}_j} = \alpha_\xi \times \frac{\partial \Phi_\sigma^\varsigma(\mathbf{U}_h)}{\partial \mathbf{U}_j} \quad (31)$$

4.4 Coincidence of quadrature formula

We now need to apply the requirements of relation (21) to the p -adaptation. In the case of an interface between two elements of the same degree, we simply use the same quadrature formula, and so the requirements of relation (21) are automatically satisfied. For an interface between a subdivided element and a non-subdivided one, we use quadrature formulas such that all the quadrature points at the interface physically coincide.

5 Numerical test cases using p -adaptation

With our residual distribution scheme compatible with subdivided elements, we present now some numerical results in the two-dimensional case.

5.1 Lax-Wendroff scheme - Subsonic test case

We show here, just for theoretical purposes, how our method behaves with a Lax-Wendroff scheme with a NACA0012 wing profile. The inflow condition is Mach=0.5, a pressure $P_{inlet} = 0.7$ and a mesh with randomly subdivided (we randomly select half of the elements of the mesh and subdivide them into \mathbb{P}^1 elements). The mesh along with the subdivided elements are shown in fig.2.

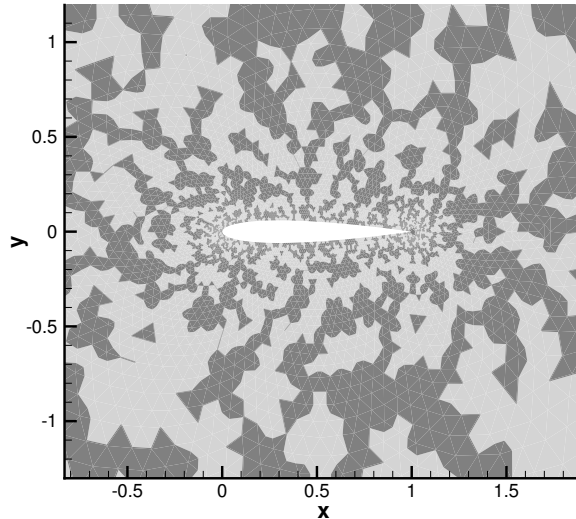


Figure 2: Mesh of Naca0012 for Problem 5.1 with elements randomly subdivided: elements in dark zones are subdivided, the others are not subdivided.

We can see, in fig.3, a comparison of the convergence curves when \mathbb{P}^1 , \mathbb{P}^2 and mixed elements (\mathbb{P}^2 elements and subdivided \mathbb{P}^1 elements) are used. We remark that with the same level of convergence for the three types of finite elements, the convergence speed with subdivided elements is as expected between those obtained with \mathbb{P}^1 and \mathbb{P}^2 elements.

As stated above, for this test case the elements are arbitrarily subdivided and we do not take advantage of p -adaptation to improve the accuracy of the solution. In the next test cases, the elements will be subdivided according to the properties of the solution.

5.2 Lax-Friedrichs scheme - Transonic test case

We test our method on a Naca0012 wing profile with Mach=0.8, a pressure of 0.71 and an angle of attack of 1.25 degrees. For this problem, we use the Lax-Friedrichs scheme, for its ability to capture the shock occurring in transonic flights.

In order to combine the robustness brought by the use of \mathbb{P}^1 elements in low regularity zones and the overall better properties of the \mathbb{P}^2 elements, we test our method with a shock capturing term that allows us to use \mathbb{P}^1 elements only where the shock is detected and \mathbb{P}^2 elements elsewhere.

5.2.1 Shock capturing term

For this purpose, we use the following shock detector (see [6]), based here on the variation of pressure:

$$\theta_K = \max_{\sigma \in K} \left(\max_{K', \sigma \in K'} \frac{|\max_{\nu \in K'} p_\nu - \min_{\nu \in K'} p_\nu|}{|\max_{\nu \in K'} p_\nu| + |\min_{\nu \in K'} p_\nu| + \epsilon} \right) \quad (32)$$

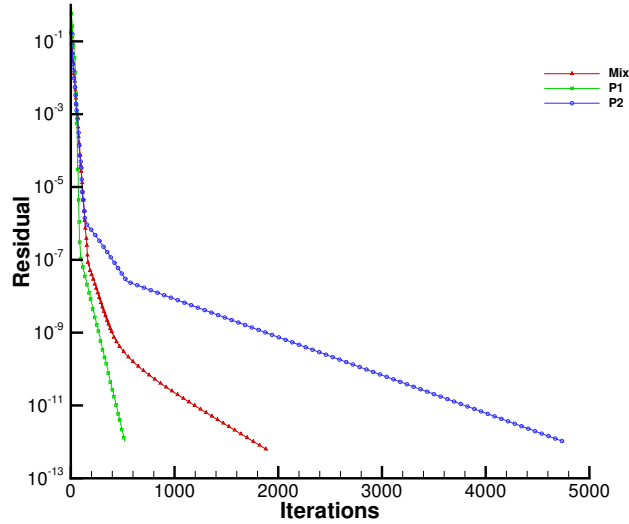


Figure 3: Convergence of residuals for test case 5.1.

where σ , ν are degrees of freedom, K and K' are elements of Ω , and ϵ is the machine epsilon (in our implementation, $\epsilon = 1e - 16$).

For this transonic speed (Mach = 0.80) and a mesh of 2355 vertices, our shock detector gives the subdivision map shown in fig.4. The subdivided elements are dark-coloured and correspond to the elements containing a strong variation of pressure.

5.2.2 Shock detector and p-adaptation

With the shock detector presented above, we test our subdivision method by applying it to the shock zone. Practically, in all the test cases presented in this paper, the shock detector is used as follows : we set a unique threshold, θ_{th} (depending on the test case), we start with subdivided elements \mathbb{P}^1 everywhere, then after a short number of iterations (this number depending on the test case), the detector θ_K is computed for each element K . If the value θ_K is above the threshold, θ_{th} , then the element remains subdivided with \mathbb{P}^1 elements, else, the element becomes a \mathbb{P}^2 element (and is not subdivided). As a result, we use \mathbb{P}^1 elements in the shock zone, and \mathbb{P}^2 elements everywhere else.

The convergence curve obtained with p -adaptation, fig. 5, shows a jump of the residual due to the switch from \mathbb{P}^1 elements to \mathbb{P}^2 elements everywhere except in the shock zone. After the jump, we observe the convergence of the residual. For our transonic test case θ_{th} was set to 1.5, and the switch was set after 300 iterations.

5.2.3 Shock width, oscillations and p-adaptation

We remark from fig. 6, that the position of the shock obtained with mixed elements is in very good agreement with the position predicted using classical \mathbb{P}^2 or \mathbb{P}^1 elements. This is important for the validation of our method and proves that we are here consistent with the results obtained

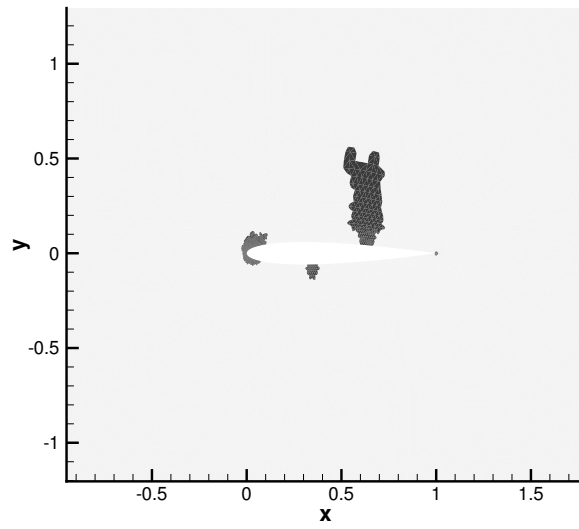


Figure 4: Shock zone for test case 5.2: subdivided elements are dark-coloured.

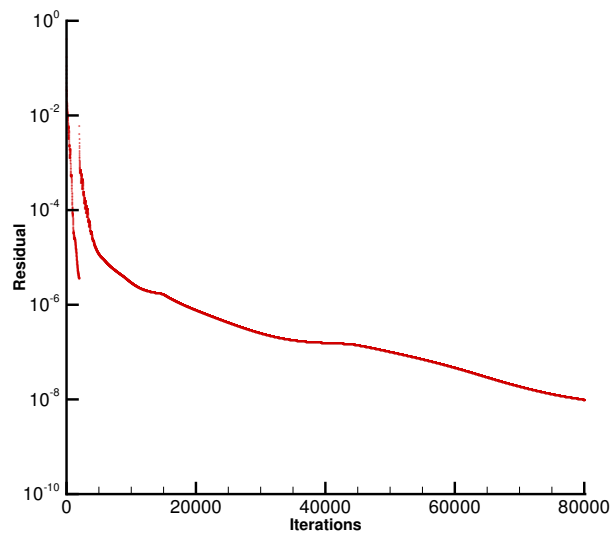


Figure 5: Convergence of residual for test case 5.2 with mixed elements.

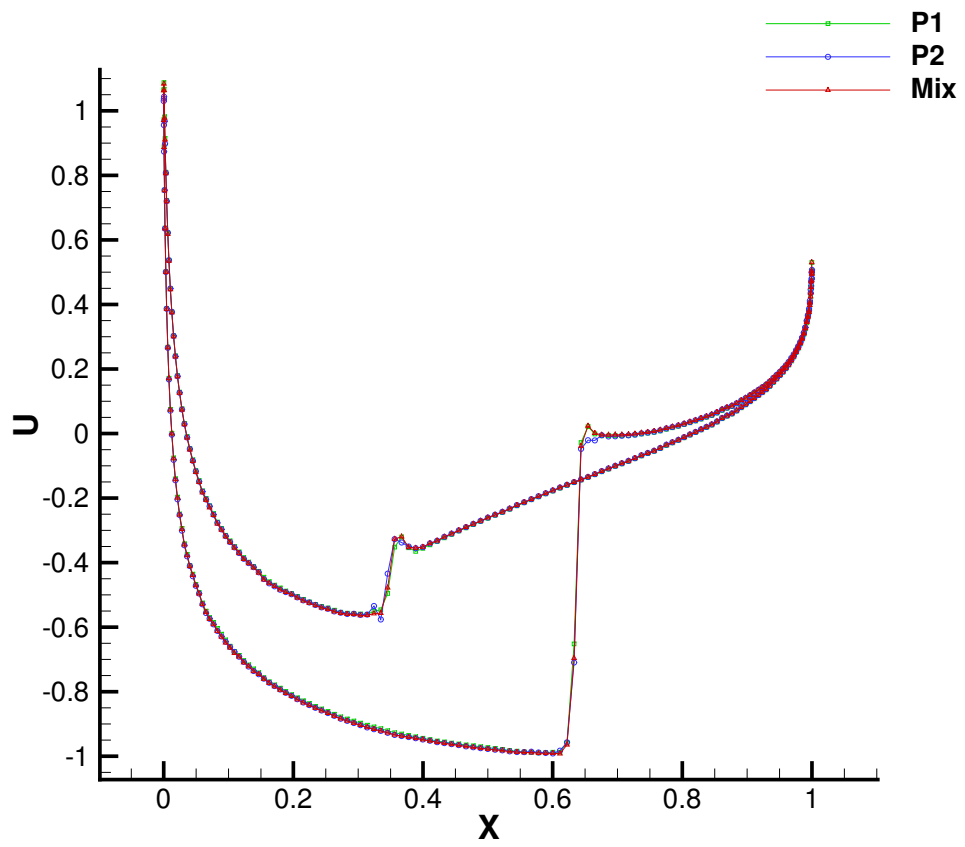
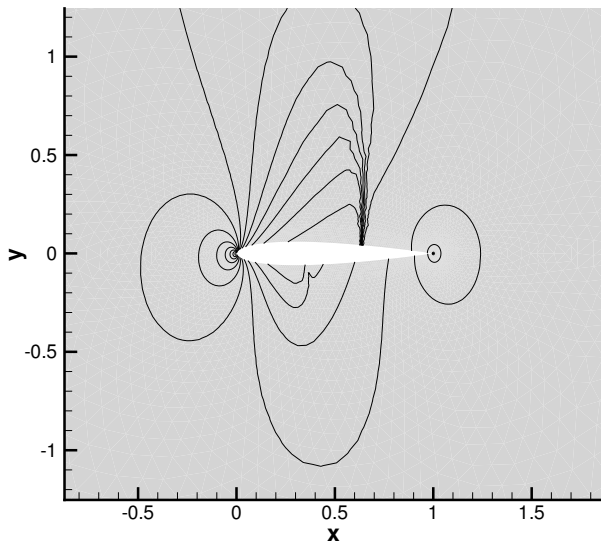
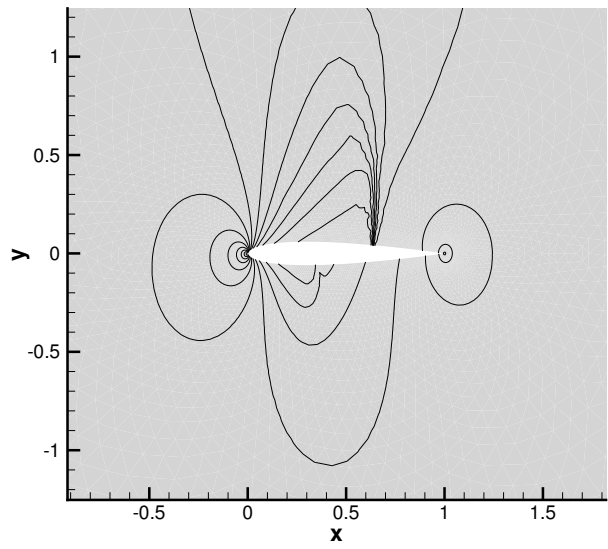


Figure 6: Comparison of pressure coefficients obtained with \mathbb{P}^1 , \mathbb{P}^2 and mixed elements.

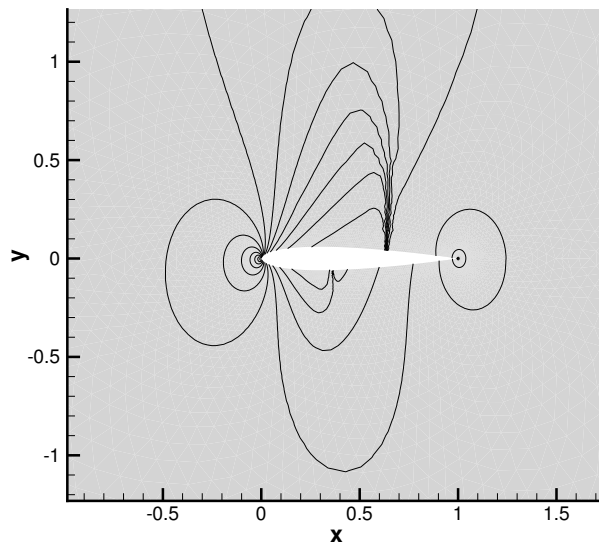
Figure 7: Comparison of solutions for test case 5.2 between \mathbb{P}^2 and mixed elements:



(a) Pressure (\mathbb{P}^1 elements)



(b) Pressure (\mathbb{P}^2 elements)



(c) Pressure (mixed elements)

with classical \mathbb{P}^1 and \mathbb{P}^2 elements. In addition, we make the following interesting observation: as we reduce the size of the elements in the shock zone by using p -adaptation (because of subdivided elements), the discontinuity occurring in the pressure coefficient is better captured than within a non subdivided element.

Furthermore, if we compare, in fig. 7, the solutions obtained with p -adaptation to the solution obtained with classical \mathbb{P}^2 elements everywhere, we can see that the former displays better shock capturing abilities, while still exhibiting the non oscillatory behavior of higher order elements in more regular zones.

5.3 Supersonic test case

Now we present a numerical test with a higher speed, Mach=3. Because of the higher speed used, such test cases can be more difficult to run. The application of p -adaptation, even to a little number of elements (only in the shock zone), allows convergence of the residual and proves to be an efficient approach to simulate such phenomenon. Since the number of sub-divided elements is small the method remains mostly \mathbb{P}^2 based.

The following parameters are set: the mesh is made of 3749 vertices and contains a sphere of diameter 1, centered in 0, which is moving at Mach=3.0.

We divide the boundary conditions into 4 sub-boundaries as shown in fig. 8, and we detail in the following the conditions applied to each of these boundaries:

- on the sphere (boundary 1) inside the domain, we impose a slipping wall boundary condition,
- in front of the sphere (boundary 2, the half circle on the left of the domain), we impose Dirichlet boundary conditions with $(\rho, u, v, p) = (1, 3, 0, 1.4)$,
- on the upper and lower horizontal lines (boundary 3), we impose a slipping wall boundary condition,
- behind the sphere (boundary 4, the vertical line at the right of the domain), we use a Steger-Warming exit boundary condition with $(\rho, u, v, p) = (1, 0.8, 0, 0.3)$.

As initial conditions we set a discontinuity line at $x = 0.435$, with $(\rho, u, v, p) = (1, 0, 0, 1.4)$ on the left of the discontinuity and $(\rho, u, v, p) = (1, 3, 0, 1.4)$ on the right.

We use the shock detector defined in 5.2.1 and the obtained map of subdivided elements dark-coloured is shown in fig. 9. We use \mathbb{P}^1 elements in the shock zone and \mathbb{P}^2 elements elsewhere, following the method described in section 5.2.2 with $\theta_{th} = 3$ and a switch after 300 iterations. Again, we notice, in fig. 10, a jump in the residual due to the change from a \mathbb{P}^1 -only scheme to a mixed \mathbb{P}^1 - \mathbb{P}^2 element scheme after the activation of the shock detector.

The obtained solution is shown in figures 11 for the isolines of the Mach number, 12 for the isolines of the pressure and 13 for the isolines of the density. As of today, we have not been able to make the classical \mathbb{P}^2 scheme converge for this test case. With p -adaptation we obtain a high-order solution that physically agrees with the solution obtained with a classical \mathbb{P}^1 scheme.

6 Extension to three dimensions

We now present the extension of p -adaptation with residual distribution schemes to solve three dimensional problems. We only present here some preliminary results, with tetrahedral elements, as the extension to 3D cases will be the subject of following papers. The important point to note is that the method presented above is fully adaptable to three dimensional problems, with

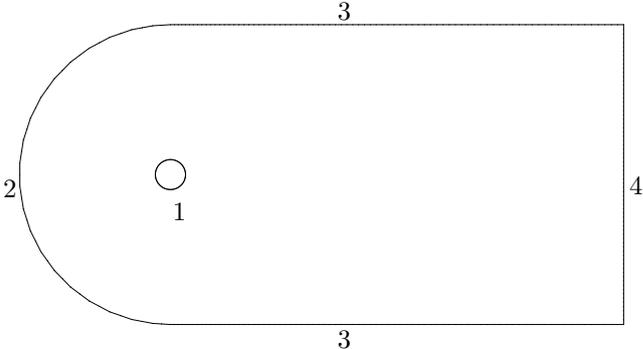


Figure 8: Boundaries for test case 5.3.

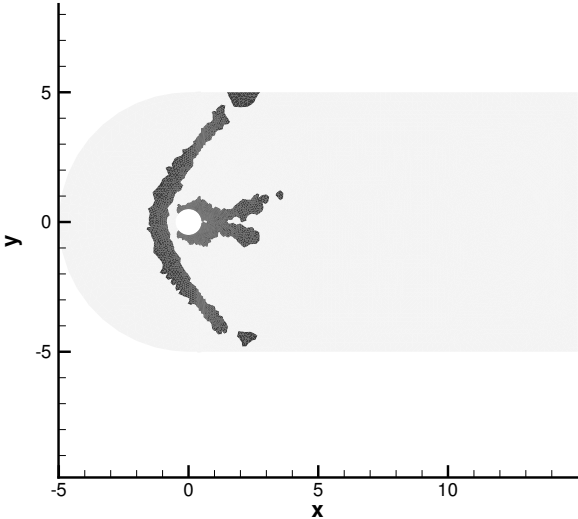


Figure 9: Shock zone for test case 5.3: subdivided elements are dark-coloured.

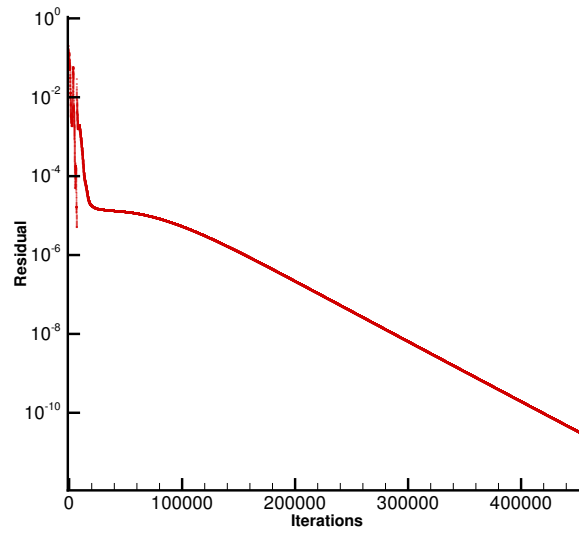


Figure 10: Convergence of residual in test case 5.3.

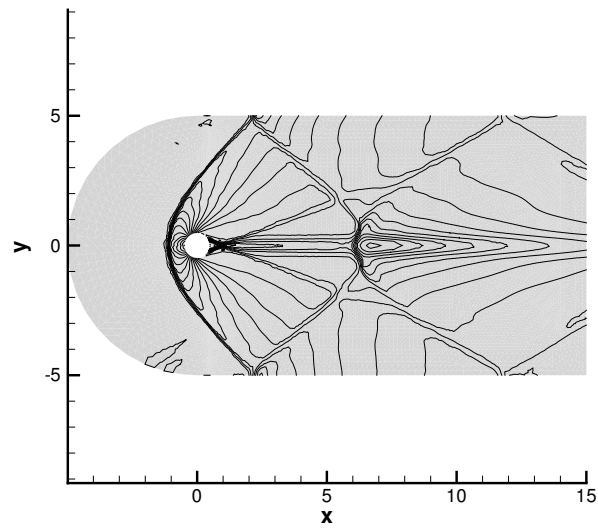


Figure 11: Mach number isolines for test case 5.3.

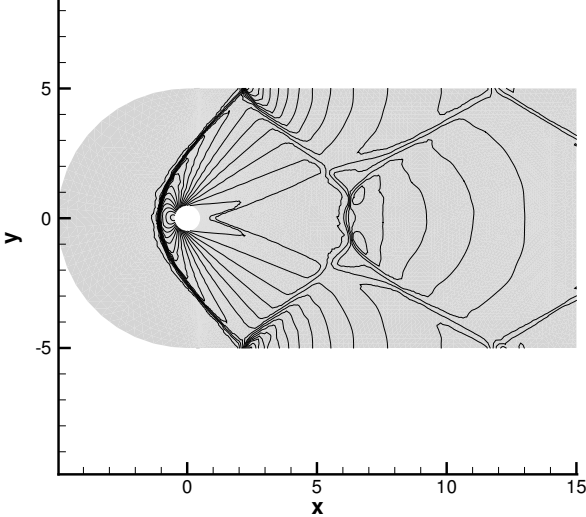


Figure 12: Pressure isolines for test case 5.3.

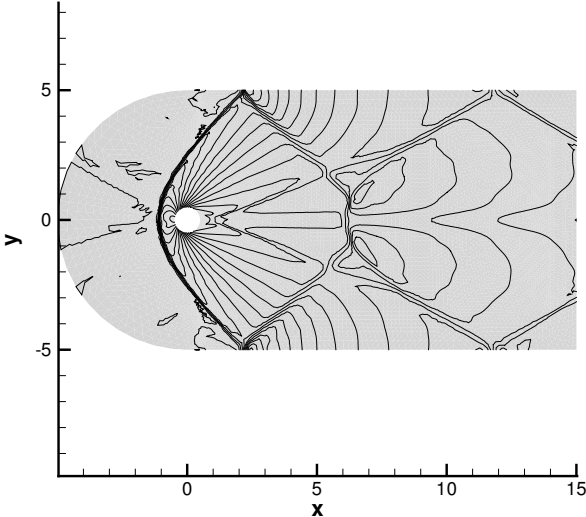


Figure 13: Density isolines for test case 5.3.

the important exception that relation (22) has no equivalent in 3D, at least if we strictly stick to Lagrange interpolation. Fortunately, this problem can be worked out, as we explain in the following.

6.1 3D p-adaptation with quadratic tetrahedra

For better clarity, we detail the reference tetrahedron and the basis functions used. For a tetrahedron K , illustrated fig. 14, we define the 10 nodes used for the subdivision. For the reference tetrahedron, the coordinates of those nodes are given by:

$$\begin{aligned} 1 &= (0, 0, 0); & 2 &= (1, 0, 0); & 3 &= (0, 0, 1); & 4 &= (0, 1, 0); \\ 5 &= (1/2, 0, 0); & 6 &= (1/2, 0, 1/2); & 7 &= (0, 0, 1/2); \\ 8 &= (1/2, 1/2, 0); & 9 &= (0, 1/2, 1/2); & 10 &= (0, 1/2, 0). \end{aligned}$$

First, we subdivide the tetrahedron into eight sub-tetrahedra as shown in fig. 14. The central octahedron (5, 6, 7, 8, 9, 10) can be split with the diagonal (7, 8), (6, 10) or (5, 9), as shown in fig. 15, and the sub-tetrahedra obtained are then:

- Exterior tetrahedra:
 $K_1 = (5, 7, 10, 1); K_2 = (2, 6, 5, 8); K_3 = (3, 9, 6, 7); K_4 = (8, 9, 10, 4),$
- With diagonal (7, 8):
 $K_5 = (6, 9, 8, 7); K_6 = (8, 9, 10, 7); K_7 = (8, 10, 5, 7); K_8 = (8, 6, 5, 7).$
- With diagonal (6, 10):
 $K_5 = (6, 9, 8, 7); K_6 = (8, 9, 10, 7); K_7 = (8, 10, 5, 7); K_8 = (8, 6, 5, 7).$
- With diagonal (5, 9):
 $K_5 = (5, 9, 6, 7); K_6 = (5, 9, 10, 7); K_7 = (5, 9, 6, 8); K_8 = (5, 9, 10, 8).$

Now if we compute the coefficients of formula (22) for the 3D case using a Lagrange interpolation, we find that the coefficients corresponding to the sub-tetrahedra K_1, K_2, K_3, K_4 are equal to 0. This is due to a property inherent to \mathbb{P}^2 Lagrange basis functions in 3D:

$$\int_K \frac{\partial \varphi_j}{\partial x_d} = 0, \quad j = 1, \dots, 4, \quad d = 1, 2, 3.$$

This implies that the nodal residuals corresponding to the vertices of the tetrahedron K will not contribute to equation (8), which may give a problematic residual scheme.

To avoid this problem, while still using quadratic elements, we use the Bézier basis functions. More precisely, instead of using a Lagrange interpolation of the flux, we approximate them using a Bézier representation. From the linear algebra point of view, this is a change of basis, but now we can get positive weights.

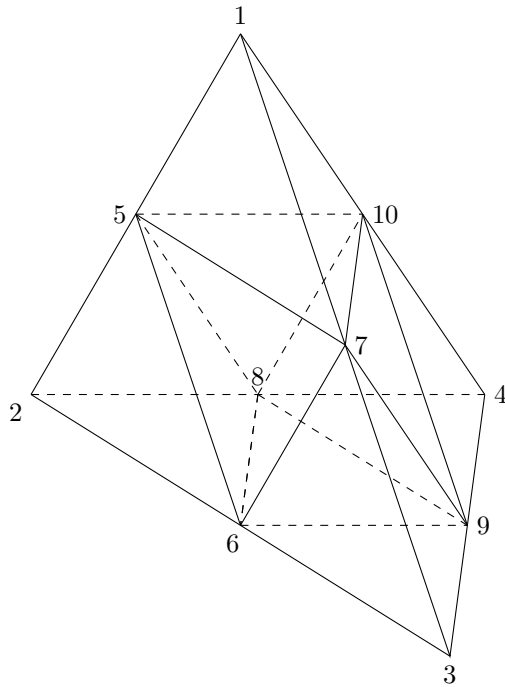


Figure 14: Subdivided tetrahedron K .

6.2 Bézier basis functions

We denote by $\lambda_\sigma, \sigma = 1, \dots, 4$ the barycentric coordinate functions in 3D, corresponding to the vertices of the tetrahedron. The Bézier basis functions are defined by:

$$\begin{aligned} B_1 &= \lambda_1^2; & B_2 &= \lambda_2^2; & B_3 &= \lambda_3^2; & B_4 &= \lambda_4^2; \\ B_5 &= 2\lambda_1\lambda_2; & B_6 &= 2\lambda_2\lambda_3; & B_7 &= 2\lambda_1\lambda_3; \\ B_8 &= 2\lambda_2\lambda_4; & B_9 &= 2\lambda_3\lambda_4; & B_{10} &= 2\lambda_1\lambda_4. \end{aligned}$$

We then have $B_\sigma \geq 0$, and $\sum_{\sigma} B_\sigma = 1$. If Φ is a quadratic polynomial, we have

$$\Phi = \sum_{\sigma=1}^{10} \Phi_\sigma B_\sigma$$

and the difference with Lagrange interpolation is that $\Phi_\sigma = \Phi(\sigma)$ only for $\sigma = 1, 2, 3, 4$. For the other degrees of freedom

$$\Phi(\sigma) = \frac{\Phi_{j_1} + \Phi_{j_2}}{4} + \frac{\Phi_\sigma}{2} \tag{33}$$

where j_1 and j_2 are the two vertices of the tetrahedron on the edge where σ lies. It is clear that $\Phi_\sigma = \Phi(\sigma) + O(h^2)$. We also notice that

$$\nabla B_\sigma = \sum_{l=1}^4 P_j^l(\lambda_1, \lambda_2, \lambda_3, \lambda_4) \nabla \lambda_j$$

where $P_j^l(\lambda_1, \lambda_2, \lambda_3, \lambda_4)$ is a polynomial in $\lambda_1, \lambda_2, \lambda_3,$ and λ_4 with *positive* coefficients.

Now we need to find an equivalent formula of (22) for the 3D case with the Bézier basis functions. In the same spirit as for (22), we expand the flux in term of Bézier polynomials:

$$\mathbf{F}^B := \sum_{\sigma=1}^{10} \mathbf{F}_\sigma B_\sigma$$

where \mathbf{F}_σ is the value of the flux at the vertices of the tetrahedron and when $\sigma > 4$ are defined according to (33).

With the notation $N_i = \nabla \lambda_i$, the gradients of the Bézier basis functions write:

$$\begin{aligned} \nabla B_1 &= 2\lambda_1 N_1; & \nabla B_2 &= 2\lambda_2 N_2; & \nabla B_3 &= 2\lambda_3 N_3; & \nabla B_4 &= 2\lambda_4 N_4; \\ \nabla B_5 &= 2(\lambda_1 N_2 + \lambda_2 N_1); & \nabla B_6 &= 2(\lambda_2 N_3 + \lambda_3 N_2); \\ \nabla B_7 &= 2(\lambda_1 N_3 + \lambda_3 N_1); & \nabla B_8 &= 2(\lambda_2 N_4 + \lambda_4 N_2); \\ \nabla B_9 &= 2(\lambda_3 N_4 + \lambda_4 N_3); & \nabla B_{10} &= 2(\lambda_1 N_4 + \lambda_4 N_1) \end{aligned} \quad (34)$$

With $\mathbf{n}_j = \int_K N_j$, we find the following formula for the 3d case:

$$\begin{aligned} 1/2 \int_K \operatorname{div} \mathbf{F}^B dx &= 1/2 \sum_{\sigma=1}^{10} \left(\int_K \mathbf{F}_\sigma \operatorname{div} B_\sigma dx \right) \\ &= (\mathbf{F}_1 \mathbf{n}_1 + \mathbf{F}_2 \mathbf{n}_2 + \mathbf{F}_3 \mathbf{n}_3 + \mathbf{F}_4 \mathbf{n}_4) \\ &\quad + (\mathbf{F}_5 \mathbf{n}_2 + \mathbf{F}_5 \mathbf{n}_1) + (\mathbf{F}_6 \mathbf{n}_3 + \mathbf{F}_6 \mathbf{n}_2) \\ &\quad + (\mathbf{F}_7 \mathbf{n}_1 + \mathbf{F}_7 \mathbf{n}_3) + (\mathbf{F}_8 \mathbf{n}_4 + \mathbf{F}_8 \mathbf{n}_2) \\ &\quad + (\mathbf{F}_9 \mathbf{n}_3 + \mathbf{F}_9 \mathbf{n}_4) + (\mathbf{F}_{10} \mathbf{n}_4 + \mathbf{F}_{10} \mathbf{n}_1) \\ &= (\mathbf{F}_1 \mathbf{n}_1 + \mathbf{F}_5 \mathbf{n}_2 + \mathbf{F}_{10} \mathbf{n}_4 + \mathbf{F}_7 \mathbf{n}_3) \quad (I) \\ &\quad + (\mathbf{F}_2 \mathbf{n}_2 + \mathbf{F}_6 \mathbf{n}_3 + \mathbf{F}_5 \mathbf{n}_1 + \mathbf{F}_8 \mathbf{n}_4) \quad (II) \\ &\quad + (\mathbf{F}_3 \mathbf{n}_3 + \mathbf{F}_9 \mathbf{n}_4 + \mathbf{F}_6 \mathbf{n}_2 + \mathbf{F}_7 \mathbf{n}_1) \quad (III) \\ &\quad + (\mathbf{F}_8 \mathbf{n}_2 + \mathbf{F}_9 \mathbf{n}_3 + \mathbf{F}_{10} \mathbf{n}_1 + \mathbf{F}_4 \mathbf{n}_4) \quad (IV) \end{aligned} \quad (35)$$

The quantities (I), (II), (III), (IV) are interpreted as the integrals of the divergence of the following one degree polynomial functions:

$$\begin{aligned} (I) &= \int_{K_1} \operatorname{div} \tilde{\mathbf{F}}^{(1)} dx \\ (II) &= \int_{K_2} \operatorname{div} \tilde{\mathbf{F}}^{(1)} dx \\ (III) &= \int_{K_3} \operatorname{div} \tilde{\mathbf{F}}^{(1)} dx \\ (IV) &= \int_{K_4} \operatorname{div} \tilde{\mathbf{F}}^{(1)} dx \end{aligned}$$

where

- On (I), $\tilde{\mathbf{F}}^{(1)} = \mathbf{F}_1 \lambda_1 + \mathbf{F}_5 \lambda_2 + \mathbf{F}_{10} \lambda_4 + \mathbf{F}_7 \lambda_3$
- On (II), $\tilde{\mathbf{F}}^{(1)} = \mathbf{F}_2 \lambda_2 + \mathbf{F}_6 \lambda_3 + \mathbf{F}_5 \lambda_1 + \mathbf{F}_8 \lambda_4$
- On (III), $\tilde{\mathbf{F}}^{(1)} = \mathbf{F}_3 \lambda_3 + \mathbf{F}_9 \lambda_4 + \mathbf{F}_6 \lambda_2 + \mathbf{F}_7 \lambda_1$
- On (IV), $\tilde{\mathbf{F}}^{(1)} = \mathbf{F}_8 \lambda_2 + \mathbf{F}_9 \lambda_3 + \mathbf{F}_{10} \lambda_1 + \mathbf{F}_4 \lambda_4$

Strictly speaking, \mathbf{F}_σ is *not* the value of the flux at the vertices of K_j , but this is not a problem, following [8].

The equality (35) shows like equality (22) a relation between the quadratic residual in K and the affine residuals in the sub-tetrahedra, with positive weights independent of the splitting of the central octahedron.

6.3 Hypersonic three dimensional test case

We present now a numerical test case with a hypersonic speed (Mach=8). The very high speed, combined with the fact that the test case is run in three dimensions, makes it a difficult and demanding test case. Like in two dimensions, the application of *p*-adaptation to a little number of elements in the shock zone (the method remaining mostly \mathbb{P}^2 based), proves practically to be efficient as it allows convergence of the residual and gives a solution that looks physically admissible.

The following parameters are set: a sphere of diameter two is centered in 0 and is moving at the speed of Mach=8. The boundary conditions are divided into four sub-boundaries, as shown in fig.16. On the sphere inside the domain (boundary 1), we impose a slipping wall boundary condition, in the left face of the domain (boundary 2), we impose a Steger-Warming entry boundary condition, with $(\rho, u, v, w, p) = (8.0, 8.25, 0.0, 0.0, 116.5)$, in the right face of the domain (boundary 3), we impose a Steger-Warming exit boundary condition, with $(\rho, u, v, w, p) = (1.4, 0.0, 0.0, 0.0, 1.0)$, and on the other faces of the boundary (boundary 4), we impose a slipping wall boundary condition. As an initial condition we set a vertical plan of discontinuity at $x = 0.09$, with $(\rho, u, v, w, p) = (8.0, 8.25, 0.0, 0.0, 116.5)$ at the left of the discontinuity, and $(\rho, u, v, w, p) = (1.4, 0.0, 0.0, 0.0, 1.0)$ at the right of the discontinuity.

As shown in fig.17, the residual converges well, even with only a very small number of \mathbb{P}^1 elements in the shock zone (see fig.18). Like in test case 5.3, with here a threshold $\theta_{th} = 8$, we start with subdivided \mathbb{P}^1 elements everywhere. After 300 iterations, only elements in the shock zone remain \mathbb{P}^1 , all the others become \mathbb{P}^2 elements. The converged solution (Mach number, pressure and density), is shown in respectively figures 19, 20 and 21.

7 Conclusion

We have described a way to use *p*-adaptation with continuous finite elements within the frame of residual distribution schemes. We have proved theoretically the validity of the method, and we have shown for complex problems modeled by the Euler equations that the method is robust for subsonic, transonic, supersonic and hypersonic flows. We have shown that our method fully extends to three dimensional cases, notably with the use of Bézier basis functions for *p*-adaptation with \mathbb{P}^1 and quadratic elements. Further applications of our method in dimension two and three will be detailed in our next publications, like the extension to higher order (cubic or more) elements and the extension to the Navier-Stokes equations.

Acknowledgments

- This study has been carried out with financial support from the French State, managed by the French National Research Agency (ANR) in the frame of the "Investments for the future" Programme IdEx Bordeaux - CPU (ANR-10-IDEX-03-02).

- Experiments presented in this paper were carried out using the cluster Avakas and the PLAFRIM experimental testbed. PLAFRIM is developed under the Inria PlaFRIM development action with support from LABRI, IMB and other entities: Conseil Régional d'Aquitaine, FeDER, Université de Bordeaux and CNRS.

A Implicit numerical solver

We need to solve the system of equations (8), written in a compact way as:

$$R(\mathbf{U}_h) = 0. \quad (36)$$

This problem is first relaxed as:

$$\frac{d\mathbf{U}_h}{dt} = -R(\mathbf{U}_h). \quad (37)$$

To approximate this time derivative, we use the backward Euler formula, and the problem becomes:

$$\frac{\mathbf{U}_h^{n+1} - \mathbf{U}_h^n}{\Delta t^n} = -R(\mathbf{U}_h^{n+1}), n = 0, 1, 2, \dots \quad (38)$$

Thus, we have to solve a non linear problem at each time step n . We use for that a Newton method, that when applied to (36) reads:

$$\mathbf{U}_h^{k+1} = \mathbf{U}_h^k - J^{-1}R(\mathbf{U}_h^k), k = 0, 1, 2, \dots \quad (39)$$

where

$$J = \frac{\partial R(\mathbf{U}_h^k)}{\partial \mathbf{U}^k} \quad (40)$$

is the Jacobian of R . In practice, the Jacobian J is computed from a first order scheme with the stabilization term. And so, with our Newton method applied to (38), the linear system we have to solve at each time step n reads:

$$\left[\frac{1}{\Delta t^n} + J(\mathbf{U}_{h_k}^n) \right] \Delta \mathbf{U}_{h_k}^n = -R(\mathbf{U}_{h_k}^n) \quad (41)$$

$$\mathbf{U}_{h_{k+1}}^n = \mathbf{U}_{h_k}^n + \Delta \mathbf{U}_{h_k}^n, k = 0, 1, 2, \dots \quad (42)$$

In practice, for each time step n , we use only one iteration on k , which seems enough to reach convergence of the nodal residuals to the zero machine.

References

- [1] Rémi Abgrall. Toward the ultimate conservative scheme: following the quest. *Journal of Computational Physics*, 167(2):277–315, 2001.
- [2] Rémi Abgrall. Essentially non-oscillatory residual distribution schemes for hyperbolic problems. *Journal of Computational Physics*, 214(2):773–808, 2006.
- [3] Rémi Abgrall. Icm 2014 Seoul. In Dae-Woong Le Sung Young Jang, Young Rock Kim and Ikkwon Yie, editors, *Proceeding of the International Congress of Mathematicians*, volume IV, pages 699–726. KM Kyong Moon SA, 2014.

-
- [4] Rémi Abgrall and Timothy Barth. Residual distribution schemes for conservation laws via adaptive quadrature. *SIAM Journal on Scientific Computing*, 24(3):732–769, 2003.
 - [5] Rémi Abgrall, Adam Larat, and Mario Ricchiuto. Non-oscillatory high-order residual distribution schemes for the euler equations. In *First symposium on Current and New Trends in Scientific Computing*, 2009.
 - [6] Rémi Abgrall, Adam Larat, and Mario Ricchiuto. Construction of very high order residual distribution schemes for steady inviscid flow problems on hybrid unstructured meshes. *Journal of Computational Physics*, 230(11):4103–4136, 2011.
 - [7] Rémi Abgrall and Philip L Roe. High order fluctuation schemes on triangular meshes. *Journal of Scientific Computing*, 19(1-3):3–36, 2003.
 - [8] Rémi Abgrall and J Treflik. An example of high order residual distribution scheme using non-lagrange elements. *Journal of Scientific Computing*, 45(1-3):3–25, 2010.
 - [9] Douglas N Arnold, Franco Brezzi, Bernardo Cockburn, and L Donatella Marini. Unified analysis of discontinuous Galerkin methods for elliptic problems. *SIAM journal on numerical analysis*, 39(5):1749–1779, 2002.
 - [10] I. Babuška and B.Q. Guo. The h, p and $h-p$ version of the finite element method; basis theory and applications. *Adv. Eng. Softw.*, 15(3-4):159–174, 1992.
 - [11] A Cangiani, J Chapman, EH Georgoulis, and M Jensen. Implementation of the continuous-discontinuous galerkin finite element method. *Numerical Mathematics and Advanced Applications 2011*, page 315.
 - [12] Juan CHENG and Chi-Wang SHU. High order schemes for cfd: A review. *Chinese Journal of Computational Physics*, 5:002, 2009.
 - [13] Dante De Santis. *Development of a high-order residual distribution method for Navier-Stokes and RANS equations*. PhD thesis, Université Sciences et Technologies - Bordeaux I, 2013.
 - [14] H Deconinck, H Paillere, R Struijs, and Philip L Roe. Multidimensional upwind schemes based on fluctuation-splitting for systems of conservation laws. *Computational Mechanics*, 11(5-6):323–340, 1993.
 - [15] Daniele Antonio Di Pietro and Alexandre Ern. *Mathematical aspects of discontinuous Galerkin methods*, volume 69. Springer Science & Business Media, 2011.
 - [16] John A Ekaterinaris. High-order accurate, low numerical diffusion methods for aerodynamics. *Progress in Aerospace Sciences*, 41(3):192–300, 2005.
 - [17] Ralf Hartmann. Discontinuous galerkin methods for compressible flows: higher order accuracy, error estimation and adaptivity. *Lecture series - Von Karman Institute for Fluid Dynamics*, 1:5, 2006.
 - [18] George Em Karniadakis, Chi-Wang Shu, and Bernardo Cockburn. *Discontinuous Galerkin Methods: Theory, Computation and Applications*. Springer, 2000.
 - [19] William F Mitchell and Marjorie A McClain. A comparison of hp-adaptive strategies for elliptic partial differential equations. *ACM Transactions on Mathematical Software (TOMS)*, 41(1):2, 2014.

-
- [20] D Moxey, MD Green, SJ Sherwin, and J Peiró. An isoparametric approach to high-order curvilinear boundary-layer meshing. *Computer Methods in Applied Mechanics and Engineering*, 283:636–650, 2015.
- [21] Mario Ricchiuto. *Contributions to the development of residual discretizations for hyperbolic conservation laws with application to shallow water flows*. Habilitation à diriger des recherches, Université Sciences et Technologies - Bordeaux I, 2011.
- [22] Khosro Shahbazi, Paul F Fischer, and C Ross Ethier. A high-order discontinuous galerkin method for the unsteady incompressible navier–stokes equations. *Journal of Computational Physics*, 222(1):391–407, 2007.
- [23] ZJ Wang. High-order methods for the euler and navier–stokes equations on unstructured grids. *Progress in Aerospace Sciences*, 43(1):1–41, 2007.
- [24] ZJ Wang. High-order computational fluid dynamics tools for aircraft design. *Philosophical transactions. Series A, Mathematical, physical, and engineering sciences*, 372(2022), 2014.
- [25] ZJ Wang, Krzysztof Fidkowski, Rémi Abgrall, Francesco Bassi, Doru Caraeni, Andrew Cary, Herman Deconinck, Ralf Hartmann, Koen Hillewaert, HT Huynh, et al. High-order cfd methods: current status and perspective. *International Journal for Numerical Methods in Fluids*, 72(8):811–845, 2013.

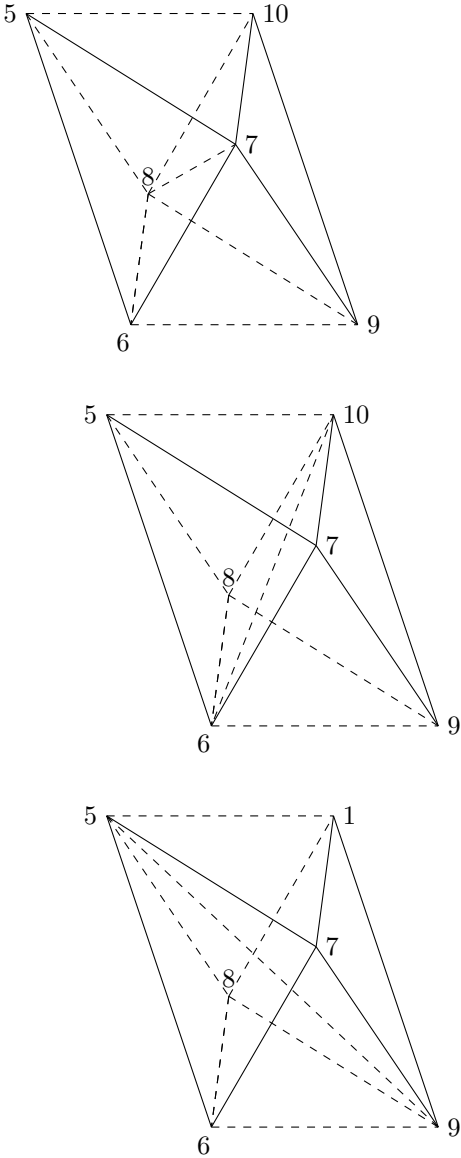


Figure 15: Subdivided octahedron with resp. diagonal (8,7),(10,6) and (5,9).

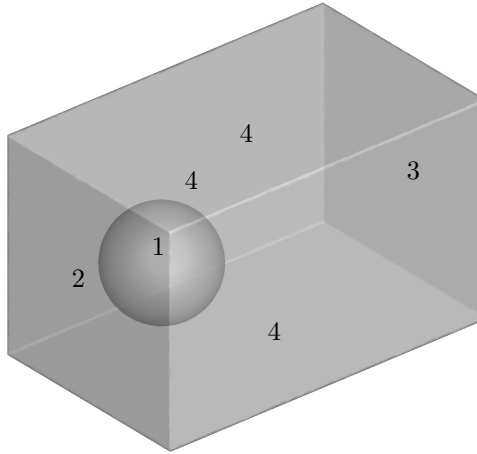


Figure 16: Boundaries for test case 6.3.

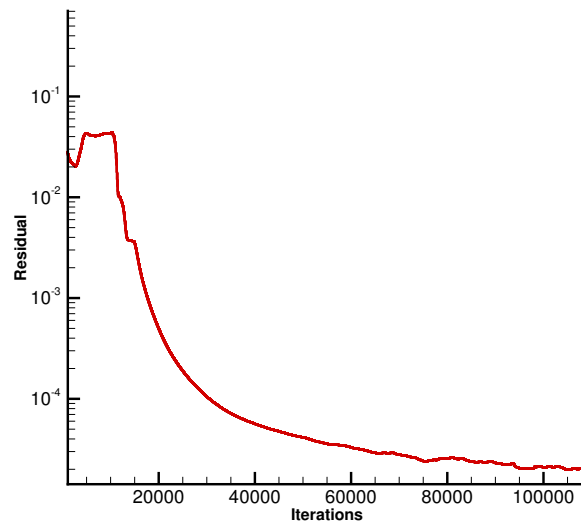


Figure 17: Convergence of residual for test case 6.3

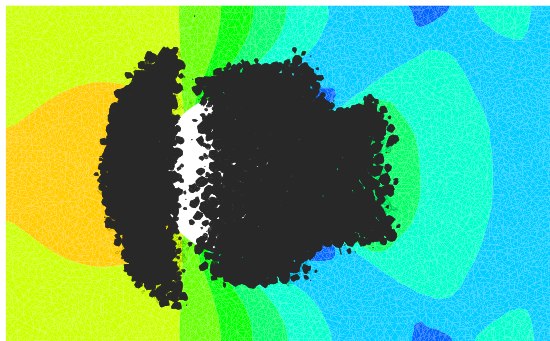


Figure 18: Shock zone for test case 6.3 (with 2d slice cut at $y = 0$ of the pressure).

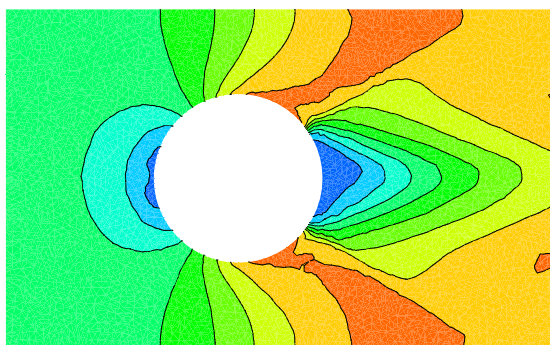


Figure 19: Mach number isolines for test case 6.3 (2d slice cut at $y = 0$).

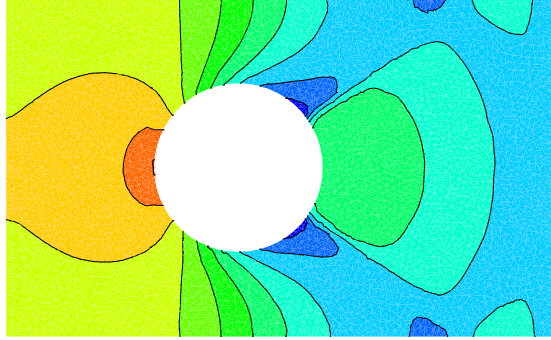


Figure 20: Pressure isolines for test case 6.3 (2d slice cut at $y = 0$).

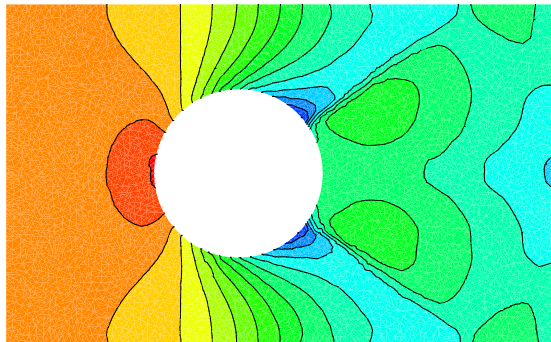


Figure 21: Density isolines for test case 6.3 (2d slice cut at $y = 0$).



**RESEARCH CENTRE
BORDEAUX – SUD-OUEST**

200 avenue de la Vieille Tour
33405 Talence Cedex

Publisher
Inria
Domaine de Voluceau - Rocquencourt
BP 105 - 78153 Le Chesnay Cedex
inria.fr

ISSN 0249-6399